

Physical Parameters and Classification of Eight Galactic Nuclei from the Second Byurakan Survey

José A. de Diego

*Instituto de Astronomía
Universidad Nacional Autónoma de México
Apartado Postal 70-264
México D.F., 04510
Mexico*

ABSTRACT

Accurate spectral parameters estimates are essential to investigate the physical conditions in AGNs. Particularly, intrinsic reddening can be estimated from the $H\alpha/H\beta$ ratio of the narrow line components. The mass of the central black hole can be obtained from the stellar velocity dispersion in the bulge, which can be estimated from the [O III] $\lambda 5007$ width, or by the relation between the AGN luminosity and the width of the broad $H\beta$ component. Two different luminosity values are important: one derived from the monochromatic 5100 \AA , and the integrated luminosity for the broad component of $H\beta$. The spectral parameters are also a fundamental key to obtain a reliable classification. Spectroscopic observations with a resolution of 4.5 \AA were performed for a sample of eight galactic nuclei extracted from the Second Byurakan Survey, and one companion galaxy of SBS 1204+505B. The EW and FWHM of the emission lines were measured, and useful line ratios and diagnostic diagrams were used for object classification and reddening estimates. Intrinsic reddening quantities were calculated for all non QSO, i.e. seven objects. Particularly the amount of reddening, $B-V$ color excess, extinction coefficient and optical depths in the V band, at $H\alpha$ and $H\beta$ wavelengths, and at 5100 \AA . The broad line region size was also estimated for seven objects, as well as the central black hole masses. Three mass estimates were usually performed for each object and compared. A peculiar line, probably He I $\lambda 5048$, is detected in the QSO SBS 1626+554. Evidence for a stratified narrow line region is found for the two narrow line Seyfert 1 galaxies included in the sample. A revised classification is proposed for two objects, and the companion galaxy of SBS 1204+505B is reported as a nuclear starburst galaxy.

Subject headings: Galaxies: active – quasars: general – Galaxies: Seyfert – Galaxies: starburst

1. Introduction

The Second Byurakan Survey (SBS) is an objective prism survey of 991[□] carried out in the 1-m Schmidt telescope of the Byurakan Observatory (Stepanian 2005). The catalogue is complete at 85% for AGNs brighter than $B = 17.5$, from which it includes 761 objects: 155 Seyfert (Sy) galaxies, 596 quasi-stellar-objects (QSO) and 10 BL Lac objects.

A considerable effort has been made to classify all the AGNs listed in the SBS. Follow-up spectroscopic observations were carried out with the 6 m telescope of the Special Astrophysical Observatory (SAO, Russia), the 4.5 m Multi-mirror Telescope (MMT, USA), the 2.6 m telescope of the Byurakan Observatory (Armenia), and the 2.1 m telescopes of the Guillermo Haro Observatory and the National Astronomical Observatory in San Pedro Martir (both in Mexico). As a rule, these follow-up observations had spectral resolutions of 5-6 or 10-11 Å over the spectral range of 3300-9000 Å (see Stepanian 2005 for further details). From the 155 Sy galaxies, 38 are classified as broad line Sy 1, 31 as narrow line Sy 1 (NLS1), 25 as Sy 1.5, 8 as Sy 1.9, 44 as Sy 2. The catalogue also includes 90 low ionization nuclear emission-line regions (LINERs), 562 starburst nuclei (SBN) and starburst galaxies (SB), 195 blue compact dwarf galaxies, and 150 H II galaxies

AGNs are classified in two types according to their optical spectra. Type 1 comprises the objects with broad permitted emission lines, and narrow permitted and forbidden lines. Type 2 consists of the objects with only narrow lines. However, in the paradigm of the Unified Model (see review by Antonucci 1993), the power source and physical conditions are thought to be inherently similar for both types of objects. The differences may arise from the amount of the intrinsic energy output, the angle of vision, and the contribution from luminous young stars.

The intrinsic energy output or luminosity depends on the physical conditions in the inner part of the AGN. Two main quantities determine the energy production rate: the mass of the central black hole (BH) and the accretion rate. Other variables, such as the BH angular momentum or the structure of the accretion disk, are of secondary importance and may be used to fine-tune the theoretical models. In the last years a strong correlation between the BH mass and the host-galaxy bulge velocity dispersion has been found for both inactive and active galaxies (Gebhardt et al. 2000; Ferrarese & Merritt 2000; Tremaine et al. 2002), which confirms the impact that the presence of the central BH has on the galaxy evolution. At the

same time, reverberation mapping studies have uncovered empirical relations between the size of the broad line region (BLR) and different estimates of the AGN luminosity (Peterson 1993; Kaspi et al. 2005).

According with the Unified Model, the viewing angle determines the observed properties of the AGN. Leaving relativistic-jet effects in radio loud AGNs aside, the Unified Model anticipates that the inner nuclear regions of AGNs are embedded inside dusty tori. The detection of broad emission lines in the polarized light of the Sy 2 galaxy NGC 1068 by Antonucci & Miller (1985) was a very convincing evidence that Sy 1 and Sy 2 galaxies are basically the same objects seen from different angles. Depending on the angle of vision, the torus may obscure the inner region. Type 1 objects are thus unobscured AGN, while Type 2 are obscured.

Classifying Type 1 AGN in different categories is to some extent less complicated than classifying Type 2 objects. The broad bands arise exclusively from the BLR of Type 1 AGNs. This has lead to more phenomenological studies of the line profiles (see review by Sulentic et al. 2000). In contrast, the lines arising from the narrow line region (NLR) often compete with the lines emitted from H II regions-like, making difficult the interpretation of the theoretical results derived from photoionization models. Evidence is growing that nuclear and star formation activities may have a common trigger, which complicates the classification process. In reality, many objects are probably misclassified because of poor quality and low resolution spectroscopic data (Véron-Cetty et al. 2001), problems to separate the broad and narrow components of the Balmer lines, and the presence of Fe II blends that interferes with the measurements of the intensity and the profile parameters of $H\beta$.

This paper initially presents spectral observations of eight SBS objects and one companion galaxy of SBS 1204+505B to investigate the intrinsic reddening, the central BH mass, the size of the BLR, and to review their classification. The term *companion* will be used hereafter exclusively to designate the companion galaxy of SBS 1204+505B reported in this paper. Any other galaxy which may be related with other SBS objects will be designed as a *neighbor*. The observations were performed as part of a follow-up program to obtain medium resolution, high signal to noise observations of the AGNs catalogued in the SBS. The remaining of the paper is arranged in the following order: §2 description of the observations; §3 data reduction; §4 presentation of the general results; §5 individual analysis of each object; and §6 a summary of the main topics discussed.

2. Observations

Spectroscopic observation with the 2.1-m telescope of the National Astronomical Observatory in San Pedro Martir (Mexico) have been carried out in April 11–14 of 2002, with the Boller & Chivens spectrophotometer, equipped with a SITE $1K \times 1K$ pixel CCD installed at the Cassegrain focus. Two spectral ranges were covered for most objects: 4800-7200 Å (or 5150-7200 Å) and 6500-8000 Å, the only exception being SBS 0944+540 which was observed in the range between 6800-9000 Å. The grating used was a 600 l mm^{-1} with blaze angle $8^\circ.63$, which yields a dispersion of 94 Å mm^{-1} at the front of the CCD. The slit width was $2''.23$, resulting in an effective instrumental spectral resolution of 4.5 Å which coincides with the instrumental broadening measured from the night sky lines. Two 1800 s exposures were obtained in each waveband for all objects. The continuum of each object was detected with a signal-to-noise (S/N) between 30 and 50.

Table 1 contains the log of observations. The columns list: (1) the SBS designation (equinox B1950), according with the IAU nomenclature (except the object referred as *companion*, which would be SBS 1204+505A but it is not included explicitly in the SBS catalogue); (2)-(3) the J2000.0 coordinates with an accuracy of $\pm 1''$; (4) B magnitude as listed in the SBS catalog, with an accuracy of about $\pm 0^m.5$ (one decimal place) or $\pm 0^m.05$ (two decimal places), except for SBS 1204+505B and its companion galaxy, for which the magnitudes were calculated from the Sloan Digitalized Sky Survey (SDSS, Data Release 5) photometric database (see the procedure used in the description of these objects in §5); (5) the redshifts; (6) absolute magnitudes M_B (see eq. 1 below); (7) the dates of observation; (8) the spectral ranges covered; and (9) the AGN spectral types.

The absolute magnitude M_B in Table 1 was calculated from the expression:

$$M_B = B - 5 \log \left[z \left(1 + \frac{z}{2} \right) \right] + 2.5(1 - \alpha) \log(1 + z) - 43.01, \quad (1)$$

for $q_0 = 0$, $H_0 = 75 \text{ km s}^{-1} \text{ Mpc}^{-1}$. A spectral index value of $\alpha=0.7$ (for a power law of the form $F_\nu \propto \nu^{-\alpha}$) was adopted for the K correction, which is negligible for the low redshift objects ($z < 0.07$).

2.1. Classification criteria

The objects have been classified according with the spectroscopic criteria outlined in Stepanian (2005). The following is a short description of these criteria which includes the galactic nuclei types considered in this paper (namely QSO, Sy galaxies, and SBN) along with

other related AGNs (for a complete description of AGN classification criteria see Stepanian 2005):

- QSO - Star-like visual images and very broad permitted emission lines. Usually these lines have a Full Width Half Maximum (FWHM) larger than 5000 km s^{-1} . The absolute magnitude $M_B = -23$ separates the QSOs from other AGNs in the SBS (see fig. 22 of Stepanian 2005).
- Sy 1 - AGNs with broad permitted Balmer lines and narrow forbidden lines. The FWHM of the Balmer broad lines is usually in the range between 1000 and 6000 km s^{-1} . The FWHM of the forbidden narrow lines are in the range between 300 and 1000 km s^{-1} (e.g. Osterbrock & Koski 1976).
- NLS1 - These AGNs were described by Osterbrock & Pogge (1985). They have narrow permitted lines only slightly broader than the forbidden lines (FWHM of $\text{H}\beta$ smaller than 2000 km s^{-1} ; Goodrich 1989). The ratio $[\text{O III}]\lambda 5007/\text{H}\beta$ smaller than 3, but exceptions are allowed if there are strong emission lines of $[\text{Fe VII}]$ and $[\text{Fe X}]$. Many NLS1 have been discovered in X-rays by ROSAT and they have generally steeper soft X-ray continuum slopes than normal Sy 1s. Many NLS1 also show rapid soft X-ray variability.
- Sy 1.5 - AGNs which have a discernible narrow H II profile superposed on a broad component (Osterbrock & Koski 1976).
- Sy 1.8 - AGNs which have relatively weak broad $\text{H}\alpha$ and $\text{H}\beta$ components, superimposed on a strong narrow component.
- Sy 1.9 - AGNs which have a relatively weak broad $\text{H}\alpha$ component, superimposed on a strong narrow component. The broad $\text{H}\beta$ component is not seen.
- Sy 2 - AGNs which have strong narrow components, but not broad components. A secondary criterion is that the $[\text{O III}]\lambda 5007/\text{H}\beta$ ratio must be equal or larger than 3.
- LINER - Low Ionized Nuclear Emission-line Region. LINERs are narrow line, low activity AGNs with line ratios $[\text{O II}]\lambda 3727/[\text{O III}]\lambda 5007 \geq 1$, and $[\text{O I}]\lambda 6300/[\text{O III}]\lambda 5007 \geq 1/3$ (Heckman 1980). Kauffmann et al. (2003) also propose a line ratio $[\text{N II}]\lambda 6584/\text{H}\alpha \geq 0.6$. Ho et al. (1997) have detected a weak broad component in some of these objects.
- SBN - These objects are spiral galaxies with a bright, blue nucleus which emits a strong narrow emission line spectrum similar to low-ionization H II regions. Balzano (1983) proposed three main criteria to separate SBN from other starburst objects: (a) strong,

narrow ($\text{FWHM} \leq 250 \text{ km s}^{-1}$), low ionization (with $[\text{O III}]/\text{H}\beta < 3$) emission lines; (b) absolute bolometric magnitudes between -17.5 and 22.5; (c) conspicuous stellar nuclei.

3. Data Reduction

Standard data reduction procedures were applied to the observations, i.e. bias subtraction, flat field, illumination and response corrections, cosmic ray removal, wavelength linearization, atmospheric extinction correction, and flux calibration, by using the IRAF package *doslit*.

The wavelength calibration was accomplished with He and Ar lines from a standard comparison lamp observed before and after each object, and with the telescope still pointing at the object to avoid changes in the calibration due to structural bending. All the spectra were flux-calibrated with standard stars observed throughout the night. Fig. 1 shows the reduced spectra for the SBS objects.

Cardelli et al. (1989) and O’Donnell (1994) have proposed the use of different polynomial empirical fits (up to order eight) for different wavelength ranges to model the galactic extinction law. As shown by the later author (see figs. 2 and 3 in O’Donnell 1994), the polynomial functions have a tendency to introduce spurious bumps and depressions depending on the order of the polynomial fit (not to mention the wild behavior of high order polynomials outside of the fitting range).

NED implements a procedure to calculate the absorption in the visible and infrared bands based on Schlegel et al. (1998), who use the procedures proposed by Cardelli et al. (1989) and O’Donnell (1994). Given the data provided by NED, a simpler fit than the high-order polynomials proposed by these authors, or even data interpolation, would be enough for correcting for galactic extinction in the limited range of the spectroscopic observations such as the ones presented in this paper.

Values for the galactic extinction estimates were obtained from NED as total absorption A_λ in magnitudes for the *UBVRIJHKL'* bands. For convenience, we will perform the galactic extinction correction in flux rather than in magnitude units. Given the absorption A_λ , it is trivial to calculate the transmittance T_λ which is defined as the ratio of the transmitted to the incident radiant power:

$$T_\lambda = 10^{-0.4A_\lambda}. \quad (2)$$

The resulting transmittance data can be fitted very well by an exponential associate

function:

$$T_\lambda = b_0 + b_1(1 - e^{-\lambda/\lambda_1}) + b_2(1 - e^{-\lambda/\lambda_2}), \quad (3)$$

were b_0 , b_1 , b_2 , λ_1 and λ_2 are the fitted parameters. With increasing wavelength, the transmittance reaches a constant (asymptotic) value of $T_\infty = 1$, hence the linear parameters have the constraint that:

$$b_0 + b_1 + b_2 = 1. \quad (4)$$

The exponential associate function produces reasonable good fits for $T_\lambda > 0.1$; this is a much lower value than the transmittances calculated for the objects included in the SBS catalog, which are located well above the galactic plane and have small amounts of galactic extinction ($T_U > 0.7$). As an example, Fig. 2 shows the exponential associate fit of the transmittance data as calculated for SBS 1136+594.

Different authors have shown their preferences for either Gaussian or Lorentzian profiles to fit the broad emission lines. The choice usually depended on the properties or the kind of AGN being considered. As a few examples, it is worth to cite Marziani et al. (2003), for whom Lorentzian functions provide a better fit for sources with a high luminosity to mass ratio, while low luminosity to mass ratio sources are best fitted by a double Gaussian; Dumont & Collin-Souffrin (1990b), Moran et al. (1996), Leighly (1999), and Véron-Cetty et al. (2001) find that many NLS1 galaxies have symmetric emission lines with Lorentzian rather than Gaussian profiles. On the other hand, Rodríguez-Ardila et al. (2000) argue that Lorentzian profiles are not suited to represent NLS1 broad emission lines. The broad emission lines analyzed in this paper have been fitted using both Gaussian and Lorentzian profiles.

Some objects show evidence of very broad extended wings to the Balmer lines. These wings do not disappear using different continuum levels and can be approximated by a logarithmic law (Blumenthal & Mathews 1975).

The narrow emission lines are well fitted using single Gaussian profiles. In some cases, the wings show a minor excess near the base and a Lorentzian profile can be fitted yielding a FWHM estimate slightly lower than the Gaussian fit, in accordance with Véron-Cetty et al. (2001). However, the values reported in this paper are always calculated using Gaussian profiles.

Strong $H\alpha$ and [N II] blends were fitted simultaneously allowing the line ratio

$[\text{N II}]\lambda 6584/[\text{N II}]\lambda 6548$ to vary (within the expected errors) between 2.7 and 3.3, instead of forcing to fulfill the theoretical value of 2.94. The same procedure was used to fit the $[\text{O III}]\lambda\lambda 4959, 5007$ lines which have a theoretical value of 2.98 (Storey & Zeippen 2000). The measured line ratios were compared with the theoretical values to check for possible unmodelled errors in the fitted spectra (particularly for objects modelled using several components for the Balmer lines, or with a strong emission of Fe II).

In order to detect He II $\lambda 4686$ and to fit the real $\text{H}\beta$ profile, Fe II subtraction was performed using a template obtained from the NLS1 galaxy IZw1 (P. Marziani, priv. comm.) whose spectrum is widely used as an Fe II template. The procedure to subtract the Fe II is the same as the one reported by Zamanov & Marziani (2002).

4. Results

Table 2 shows the rest frame equivalent width (EW) in \AA and the full width half maximum (FWHM) in km s^{-1} for the observed lines in each object. These quantities have been calculated using the following expressions:

$$\text{EW} = \frac{F_l}{(1+z)F_c}, \quad (5)$$

where F_l and F_c are the observed fluxes of the line and the continuum, respectively, and

$$\text{FWHM} = \frac{c}{1+z} \frac{\Delta\lambda_{obs}}{\lambda_e}, \quad (6)$$

where c is the speed of light, $\Delta\lambda_{obs}$ is the observed FWHM in \AA , and λ_e the rest frame wavelength of the line.

The first column in Table 2 identifies the emission line, and columns 2-19 alternatively the EW in \AA and the FWHM in km s^{-1} for each object. In some cases, the spectra show a small feature that strongly suggests the existence of a known line, but the S/N ratio is below the detection level (3σ). For these features, the parameters of the fit are not accurate, and therefore their EW are indicated as superior limits, and no FWHM value is available.

The fluxes for the iron blends between 4400-4680 \AA (Fe II $\lambda 4540$), and 5100-5500 \AA (Fe II $\lambda 5300$) have been calculated from the iron template. The FWHM data were corrected for instrumental broadening (4.5 \AA).

The discussion will be centered on the Gaussian fits, although the parameters of the

Lorentzian fits were also calculated for all the permitted lines. Table 3 lists the Lorentzian parameters for those object for which the Lorentzian fits reproduce the Balmer profiles using less components than the Gaussian fits. In these cases, a single component was used except for the QSO SBS 0944+540. For this object, the simplest accurate fit was obtained using two broad Lorentzian components. Otherwise, the structure of Table 3 is similar to Table 2.

4.1. Narrow lines and diagnostic diagrams

From Table 2 it is evident that for most objects there are manifest differences between the FWHM of the lines found in the $H\beta$ and $H\alpha$ regions (SBS 0848+526, 1118+541, 1204+505B and its companion, and 1340+569), and between the narrow components of the permitted lines and the forbidden lines FWHM (SBS 1118+541 and 1136+595), and even among the forbidden lines (SBS 1118+541). The correlation between the line widths and both the critical density and the ionization potential are well known effects that can explain these differences (e.g. Pelat et al. 1981; Filippenko & Halpern 1984; de Robertis & Osterbrock 1984; Espey et al. 1994). Filippenko & Sargent (1985) find that $[O\ I]\lambda 6300$ in many LINER galaxies was broader than the $[S\ II]\lambda\lambda 6716, 6731$ lines, which they explain in terms of the different critical densities $n_e(\text{crit})$ for collisional de-excitation for these lines. Following this line of thought, the critical densities for the $[Fe\ VII]$ and $[Fe\ X]$ ions are $3.6 \times 10^7 \text{cm}^{-3}$ and $4.8 \times 10^9 \text{cm}^{-3}$, respectively. These critical densities are much higher than the mean density in the NLR, and the former lies even close to the density in the BLR. The high critical densities may explain the large FWHM values measured for these lines in some objects (SBS 1118+541 and 1340+569; see Table 2 and the discussion in §5).

The widths of the narrow lines are probably virial in their origin. For example, Nelson & Whittle (1996) have found a very good correlation between the width of the $[O\ III]$ and the stellar velocity dispersion within the bulge. The virial origin for the width of the narrow lines, along with the correlation between these widths and both the critical density and the ionization potential reviewed above, imply a radial stratification of the NLR.

Table 4 lists the emission line ratios for objects that show clear narrow Balmer components. For the objects classified as QSO, no narrow component was necessary to fit the Balmer lines, thus they are not included in the table. The line ratios have been corrected from galactic extinction. Column 1 identifies the SBS object, and columns 2-6 list the corresponding line ratio with respect to the narrow component either of $H\alpha$ or $H\beta$. Detection limits for some line ratios involving forbidden lines ($[O\ III]$, $[O\ I]$ and $[N\ II]$) have been calculated and plotted in the diagnostic diagrams (see below). Note that for SBS 0848+526 and SBS 1340+569, the $[S\ II]\ \lambda 6717$ line is outside the spectral range of the observations.

Emission line models for AGNs have led to search for diagnostic line-intensity ratios to analyze the observed optical spectra of AGNs and separate them from star-forming regions. Baldwin et al. (1981) proposed a set of empirical diagnostic diagrams which, after revisions by Osterbrock & Pogge (1985) and Veilleux & Osterbrock (1987), are the most currently used. The physics behind these diagrams is that the presence of free electrons generated by X-ray photoionization in partially ionized zones will enhance the strengths of the forbidden low-excitation lines (particularly [O I], [S II] and [N II]) produced by collisional excitation with respect to Balmer lines in narrow line AGNs, in comparison with H II region nuclei. Besides, O III is produced by hard ultraviolet photons, relatively more abundant in the AGN power law spectra than in H II regions. Thus, [O III] is an indicator of the mean level of ionization and temperature, and it is enhanced by photoionization from the harder AGN continua. This makes of [O III]/H β an excellent indicator of the AGN activity, and all the diagnostic diagrams in the optical range include this line ratio.

Kewley et al. (2001, 2006) have derived the first purely theoretical classification scheme. The relevant narrow line ratios for diagnostic diagrams are plotted in Fig. 3, along with graphs generated from Kewley et al.

4.2. Reddening

Solving the case B equation for the equilibrium level population at temperature 10^4 K and electronic density 10^4 cm $^{-3}$ for H II regions yields a ratio for the Balmer recombination decrement H α /H β of 2.85 (Osterbrock 1989). Gaskell & Ferland (1984) has shown that this ratio depends weakly on the electron density, but on the metallicity and the presence of a strong X-ray continuum. The intrinsic value for the NLR has been proposed to be 3.1 (Gaskell 1982; Gaskell & Ferland 1984; Halpern & Steiner 1983), and larger observed values are imputed to reddening by dust. As it is usual in AGN, all the H α /H β line ratios shown in Table 4 are larger than the fiducial and proposed values of 2.85 and 3.1, respectively. However it is worth to remark that dust might be not the only responsible for large H α /H β line ratios. Netzer (1982) has argued that transfer effects, self-absorption and collisional excitation of hydrogen lines are important in the BLR (which renders the broad lines unreliable for reddening measurements) and they may also have observable consequences in the NLR, affecting the Ly α /H β and H α /H β ratios (Binette et al. 1993).

Witt et al. (1992) have shown that heavily reddened components may have a negligible contribution to the total reddening, and that 'bluing' due to scattering partially compensates for reddening by extinction. Thus, to estimate the intrinsic reddening by dust within the host galaxy, we will assume that the local reddening has a continuous distribution along

the line of sight. Besides, we will also assume that the optical properties of the dust in emission line galaxies are the same than the properties of dust in the solar neighborhood (Savage & Mathis 1979). Thus, the magnitudes for the unreddened and the observed fluxes (I and F , respectively) are related by:

$$-2.5 \log I_\lambda = -2.5 \log F_\lambda - C \frac{A_\lambda}{A_V} \quad (7)$$

where C depends on the reddening and A_λ/A_V is the extinction coefficient with V normalization.

Applying eq. 7 to the observed and intrinsic fluxes for $H\alpha$ and $H\beta$, we obtain:

$$C = 2.5 \left(\frac{A_\beta - A_\alpha}{A_V} \right)^{-1} \left(\log \frac{F_\alpha}{F_\beta} - \log \frac{I_\alpha}{I_\beta} \right) \quad (8)$$

where $A_\alpha/A_V = 0.80$ and $A_\beta/A_V = 1.19$ (we will also adopt $A_B/A_V = 1.33$ and $A_{5100\text{\AA}}/A_V = 1.11$ hereafter). To calculate C , we assume the intrinsic value of $I_\alpha/I_\beta = 3.1$ for the unreddened $H\alpha/H\beta$ ratio.

Other interesting parameters can be also derived, such as the $B-V$ color excess E_{B-V} (recall that A_B/A_V is the given quantity, rather than A_B and A_V), the absorption coefficient A_V (Whittet 1992), and the optical depth τ_λ at any wavelength:

$$E_{B-V} = C \left(\frac{A_B}{A_V} - 1 \right), \quad (9)$$

$$A_V = 3.05 E_{B-V}, \quad (10)$$

$$\tau_\lambda = \frac{A_\lambda}{2.5 \log e}. \quad (11)$$

Table 5 lists all the significant reddening parameters of the NLR for the objects presented in this paper. The columns indicate: (1) the object designation; (2) the reddening constant C (eq. 8); (3) the color excess E_{B-V} (eq. 9); (4) the extinction in the V band (eq. 10); and (5), (6) (7) and (8) the optical depths (eq. 11) for the V band, $H\alpha$, $H\beta$ and at $\lambda = 5100 \text{ \AA}$.

4.3. Mass of the central black hole

Kinematic and reverberation mapping studies have lead to the finding of a strong correlation between the central black hole masses (M_{BH}) and the bulge stellar velocity dispersion

(σ). This correlation has been studied by several authors and it has been shown to be valid for both, AGN and non AGN galaxies (e.g. Ferrarese & Merritt 2000; Ferrarese et al. 2001; Gebhardt et al. 2000). Tremaine et al. (2002) have proposed the expression:

$$M_{\text{BH}} = 10^{8.13} \left(\frac{\sigma}{200 \text{ km s}^{-1}} \right)^{4.02} M_{\odot}. \quad (12)$$

Nelson & Whittle (1996) and Nelson (2000) assumed that for most AGN the forbidden line kinematics is dominated by virial motion in the host galaxy bulge, finding that the bulge velocity dispersion can be estimated from the width of the [O III] line:

$$\sigma = \frac{\text{FWHM}([\text{O III}])}{2.35}. \quad (13)$$

However, there is evidence that the use of FWHM([O III]) as an estimator of the bulge stellar velocity dispersion in AGN tends to produce large scatters and may fail for individual objects (see discussion by Onken et al. 2004).

On the other hand, Kaspi et al. (2000) monitored a sample of 28 Palomar-Green quasars for reverberation mapping and found a correlation between the size of the BLR and the luminosity at $\lambda = 5100 \text{ \AA}$, which was later updated (Kaspi et al. 2005) to the relation:

$$R_{\text{BLR}} = 22.3 \left(\frac{\lambda L_{\lambda}}{10^{44} \text{ erg s}^{-1}} \right)^{0.69} \text{ light days}. \quad (14)$$

This expression relies on the AGN continuum monochromatic luminosity at 5100 \AA which is a good approximation in the case of QSO, although for other AGN the host galaxy contribution at this wavelength can be very important. Kaspi et al. (2005) propose other possible BLR size and luminosity relations. In particular, the relation with the luminosity of the $\text{H}\beta$ broad component seems to be as accurate as with the luminosity at 5100 \AA and both power law fits share the same exponent. Furthermore, it has the advantage that the estimate for the luminosity of the broad component of $\text{H}\beta$ is not contaminated by the host galaxy. Following the same procedure as Kaspi et al. (2005) to obtain the parameters in eq. 14 (i.e. averaging the parameter values obtained from the linear regression method and from the bivariate correlated errors and intrinsic scatter), we obtain an expression that relates the BLR size with the luminosity of the broad component of $\text{H}\beta$:

$$R_{\text{BLR}} = 85.6 \left(\frac{L_{\text{H}\beta}}{10^{43} \text{ erg s}^{-1}} \right)^{0.69} \text{ light days}. \quad (15)$$

Assuming that the $H\beta$ widths indicate the random orbits of the BLR material moving with Keplerian velocity:

$$V = \frac{\sqrt{3}}{2} \text{FWHM}(H\beta) \quad (16)$$

the black hole mass can be expressed as:

$$M_{\text{BH}} = R_{\text{BLR}} V^2 G^{-1} \quad (17)$$

where G^{-1} is the gravitational constant.

Note that Onken et al. (2004) has proposed that the kinematics and geometry of the BLR introduce a scaling factor of $f = 5.5$ multiplying the mass. This factor has not been introduced in the analysis.

Table 6 lists the relevant parameters for the black holes. Column (1) identifies the object; (2) and (3) show the logarithm of the luminosities in solar units of the continuum at 5100 Å and for the $H\beta$ broadest line component, respectively, corrected by galactic extinction and intrinsic reddening when available; (4) and (5) the size of the BLR in light days calculated from the luminosities at 5100 Å and from the broadest $H\beta$ component (eqs. 14 and 15), respectively; (6), (7) and (8) the logarithms of the mass of the black hole in solar units; the first two estimates were calculated through the size of the BLR listed in columns (4) and (5) (eq. 17), and the orbital velocity of the BLR clouds estimated from the width of the broadest $H\beta$ component (eq. 16); the last mass was estimated from the width of the [O III] (eqs. 12 and 13); finally, column (9) compares the mass estimates listed in columns 6 and 8.

From the values listed in Table 6, the BH masses calculated from the kinematics (FWHM) of the broadest component of $H\beta$ and the energy output of the BLR, using either the monochromatic luminosity at 5100 Å or the luminosity of the broadest $H\beta$ component (Kaspi et al. 2005), are very consistent (the largest discrepancy, for SBS 1340+569, is only a factor 2.5). However, the comparison of these two estimates with the BH mass calculated from the velocity dispersion in the galactic bulge (Tremaine et al. 2002), estimated from the $\text{FWHM}([\text{O III}])$, shows significantly larger discrepancies (a factor of 44 for SBS 1136+594), as displayed in the last column of Table 6.

5. Notes on individual objects

5.1. SBS 0848+526

This emission line object is an X-ray (ROSAT), radio (FIRST) and infrared (2MASS) source. The host galaxy is aligned roughly in the NS direction, and it has a brighter neighbor (around 0^m5) separated by $14''$ to the NE (see description below). The SDSS image shows that the two objects have bright nuclei, and a plume extending between both galaxies, approximately aligned in the EW direction, which coincides with the slit alignment during the observations. Thus, it was possible to detect extended emission of $H\alpha$, $H\beta$ and $[O III]$ along this plume. Hence, the pair of objects seems to be another case of nuclear activity (either star formation and/or AGN) triggered by galaxy interaction.

The spectra obtained of the SBS object show only narrow lines. It is worth noticing that the $H\alpha/H\beta$ ratio for this object is large (see Table 4), which indicates a substantial reddening, with an intrinsic extinction coefficient of $A_V = 2.22$ (see Table 5).

Besides $H\alpha$ and $H\beta$, the permitted He I $\lambda 5816$ line is also observed. For the forbidden lines, the spectrum shows the $[O III] \lambda\lambda 4959, 5007$ and the $[N II] \lambda\lambda 6548, 6584$ lines, as well as a weak $[O I] \lambda 6300$. The luminosity of this SBS object is $M_B = -19.9$, the line ratio $[O III]/H\beta = 1.41$, and the $FWHM < 250 \text{ km s}^{-1}$ for all the emission lines. Hence, following Balzano (1983), the object is correctly classified in the SBS catalogue as a SBN by its optical properties. In Fig. 3 we see that the available line ratios for this object also agree with an H II region-like.

The classification of SBS 0848+526 as a SBN is also compatible with the soft X-ray emission detected by ROSAT. However, AGNs also emit in soft X-rays, which sometimes can be detected even in the case of significantly reddened objects. Recently Jiménez-Bailón et al. (2003, 2005) have studied the contribution of nuclear starbursts to the X-ray emission from AGNs. Different approaches to disentangle the origin of the X-ray emission consist on careful modelling of the starburst and AGN emissions, higher X-ray imaging resolution than the data available from ROSAT All Sky Survey ($25''$), and hard X-ray observations.

As mentioned above, the SBS object has a neighbor galaxy. This galaxy is also an X-ray source (ROSAT). It is not included in the sample presented in this paper, but a few properties may be easily inferred from the SDSS data. The SDSS spectrum of the neighbor galaxy shows several emission lines (Balmer series, Fe II blends, $[O III]$, $[O I]$, $[N II]$ - $H\alpha$ blend, and $[S II]$) at the same redshift (within the errors) as SBS 0848+526. This spectrum also shows the presence of the Fe II blends, which are usually associated with the accretion disk (e.g. Dumont & Collin-Souffrin 1990a,b). Besides, $H\alpha$ and $H\beta$ show evidence for a very

weak broad component. Thus the most probable classification for this neighbor is as a Sy 1.8 galaxy.

5.2. SBS 0944+540

This is a well known QSO (e.g. Véron-Cetty et al. 2001; Hewitt & Burbidge 1989) and a radio weak source (Bischof & Becker 1997). It shows strong emission of Fe II blends. After subtracting the Fe II emission, there is evidence for a weak He II $\lambda 4686$ emission. Although the spectrum at the red end is noisy, it shows a weak increase near 8750 \AA , which corresponds to the He I $\lambda 5876$ emission line. This line is clearly detected on the SDSS spectrum. Neither forbidden lines nor narrow components of permitted lines are observed.

The $H\beta$ profile is very asymmetric and shows a strong blue bump. This line can be fitted using either two broad Lorentzian or three broad Gaussian profiles. In the later case, two broad components ($\text{FWHM} \approx 2500 \text{ km s}^{-1}$), and a very broad component for the extended wings ($\approx 13,000 \text{ km s}^{-1}$) are necessary. These wings can also be approximated using a logarithmic law. The BH mass estimated from the widest component of $H\beta$ is approximately $6 \times 10^9 M_{\odot}$ and the BLR has a diameter of 200 light days (see Table 6).

5.3. SBS 1118+541

This object is a ROSAT and FIRST source. It has been classified as a Sy 1 by Stepanian et al. (2002), but appears as a NLS1 in the SBS catalogue. The permitted lines can be fitted using either Gaussian or Lorentzian profiles. In the cases of $H\alpha$ and $H\beta$, two Gaussian components are necessary to fit the lines, but a single Lorentzian can also reproduce their profiles. The Lorentzian profiles for the Balmer lines have a FWHM of $1400\text{-}1500 \text{ km s}^{-1}$, which are in accordance with the NLS1 classification. In the case of the Gaussian profiles, the broad components have FWHM in the range $3000\text{-}4000 \text{ km s}^{-1}$, while the narrower components are broader than the forbidden lines [$\text{FWHM}(H\beta_n) \approx 1000 \text{ km s}^{-1}$ but $\text{FWHM}([\text{O III}] \lambda\lambda 4959, 5007) \approx 540 \text{ km s}^{-1}$]. Dietrich et al. (2005) studied 12 NLS1 and also found that the Gaussian decomposition of $H\beta$ yielded broad components ($\text{FWHM} = 3275 \pm 800 \text{ km s}^{-1}$) and intermediate broad component ($\text{FWHM} = 1200 \pm 300 \text{ km s}^{-1}$).

The He II $\lambda 4686$ emission line can be easily distinguished and measured after subtracting the intense Fe II background. Fig. 4 shows the spectral region around $H\beta$ before and after subtracting the Fe II blends. The He II $\lambda 4686$ has acquired special relevance in reverberation mapping studies because it responds with negligible delay to continuum variations (e.g.

Ulrich & Horne 1996). With respect to the He I $\lambda 5876$ line, it is possible to discern between the broad and narrow components. The parameters of the broad component (EW and FWHM), which depend on the baseline adopted for the subtraction of the continuum, are relatively inaccurate, but the narrow component is relatively free of this dependency, and it shows a FWHM comparable with $H\alpha$ and $H\beta$.

The narrow components of the permitted lines are much wider than the forbidden lines observed, with the exception of the weak [Fe VII] $\lambda 6087$ and [Fe X] $\lambda 6374$. Thus, the [O III] $\lambda\lambda 4959, 5007$ and the weak lines of [O I] $\lambda 6300$ and [S II] $\lambda\lambda 6717, 6731$ have FWHM approximately half of the narrow $H\beta$ and $H\alpha$, respectively. But the forbidden lines also show a large dispersion in their FWHM, from approximately 1000 km s^{-1} of [Fe VII] to 400 km s^{-1} of [S II] $\lambda 6717$. The [N II] $\lambda\lambda 6548, 6584$ lines are not observed, probably blended with the relatively intense $H\alpha$ emission.

The Lorentzian FWHM, along with the strong Fe II blends, the presence of [Fe VII] and [Fe X], the line ratio [O III]/ $H\beta < 3$, and the X-ray emission are in accordance with the SBS classification as a NLS1. However, it is worth to note that the Gaussian analysis shows a $H\beta$ broad component (FWHM($H\beta$)= 2630 km s^{-1}) significantly wider than the nominal NLS1 limit (FWHM($H\beta$)= 2000 km s^{-1}). Separating the Balmer lines in a broad and a narrow component has led to a revision of the quality of several objects which were previously misclassified as NLS1 (e.g. Véron-Cetty et al. 2001; Botte et al. 2005; Bian et al. 2006a,b). These misclassifications were in part favored by the original definition of NLS1, which did not take into consideration the impact of a varying mix of the broad and narrow line components (Osterbrock & Pogge 1985; Goodrich 1989).

The EW of the broad and the narrow components of the Balmer lines (Table 2) can be used to compare the proportion of the flux arising from the BLR with the flux from the NLR. In this case, the BLR output is about twice the emission from the NLR. The narrow components $H\alpha/H\beta$ ratio (3.71) is moderate for a broad line AGN. Assuming a continuous distribution of local reddening, this ratio yields an intrinsic extinction coefficient of $A_V = 0.42$ and small optical depths which indicate that the object is optically thin for dust scattering in the optical bands (see Table 5).

The line ratios lie in the H II region of the diagnostic diagrams (Fig. 3). Veilleux & Osterbrock (1987) have already noted that when a Gaussian profile is used for fitting the broad Balmer components of NLS1 galaxies, the line ratios show a significant spread in the diagnostic diagrams. Hence, rather than an indication of SBN activity, this effect is the result of comparing the forbidden lines arising from the NLR with the narrow Balmer components which in this case originate in an intermediate region between the BLR and the NLR.

The differences in line widths among the forbidden lines as compared with the permitted narrow lines indicate a strong stratification of the NLR. Wilson & Heckman (1985) have discussed that the FWHM of an emission line approximately represents the bulk motion of clouds whose density is equal to the critical density for that line (cf. Ferguson et al. 1997). Filippenko & Sargent (1988) used this approximation to show that the NLR of the Sy1 nucleus M81 might be stratified, with a dependence such that the velocities v of the clouds scale as $v \propto n_e^{0.10 \pm 0.03}$. The dependency between the critical densities (for a temperature of 10^4 K) and the FWHM of the forbidden lines is shown in Fig. 5. In the case of SBS 1118+541 the weighted, linear least-squares fit shows that $v \propto n_e^{0.07 \pm 0.01}$.

Maybe the AGN spatial orientation (NLS1 are presumed to be seen face-on) permits to observe the different strata. Besides, the small amount of reddening inferred for this object (Table 5) does not impede the observation of the deeper regions. Of course, such small reddening is also in accordance with the face-on view and the presumed distribution of the dust in a torus. Ferguson et al. (1997) have shown that that the integrated narrow-line spectrum in Sy galaxies can be explained by considering an ensemble of clouds in the context of the Locally Optimally emitting Cloud (LOC) model (Baldwin et al. 1995). Under the assumption of a Keplerian gravitational velocity field, this model can predict the observed line width as a function of the critical density.

The relevant BH parameters for this object are listed in Table 6. The mass estimated from the [O III] is slightly larger but compatible with the mass estimated from the broad component of $H\beta$, and both are larger than the value expected for a NLS1 ($M_{\text{BH}} \sim 10^7 M_{\odot}$). This result counterpoints with Bian & Zhao (2004) who have investigated the BH-bulge relation in AGN. These authors found that, in the case of NLS1, the BH mass estimated from [O III] can be one order of magnitude larger than the mass estimated from $H\beta$ (see their Fig. 2). They used the 150 NLS1 sample extracted from the SDSS by Williams et al. (2002), who developed a procedure to measure the width of the whole line halfway between the fitted continuum and the line peak from the SDSS spectra. Hence, the disagreement is a result of the methodology used to measure the FWHM, and can be easily resolved applying Lorentzian rather than Gaussian fits. Thus, using the $H\beta$ FWHM listed in Table 3, the logarithm of the BH mass in solar units calculated from the continuum at 5100 \AA changes from 8.19 to 7.32. This mass is in accordance with the expected value for a NLS1 and just an order of magnitude smaller than the mass calculated from the [O III] FWHM, in agreement with Bian & Zhao (2004). The large discrepancy (a factor 7) between the BH masses inferred from line fits using Gaussian versus Lorentzian models is sobering, showing that much of the energy is in the line wings and suggesting that many BH mass estimates presented in the literature may have large and probably systematic errors.

5.4. SBS 1136+594

This AGN is a ROSAT and 2MASS source. It is classified as a Sy 1.5 galaxy in the SBS catalogue and by Gonçalves et al. (1999). The [N II] lines are very weak ($[\text{N II}]/\text{H}\alpha = 0.2$), a characteristic already reported by Martel & Osterbrock (1994) and Gonçalves et al. (1999) ($[\text{N II}]/\text{H}\alpha = 0.25$ and 0.1 , respectively). The $\text{H}\beta$ and $\text{H}\alpha$ lines show moderate asymmetric profiles (Gonçalves et al. use three components to fit $\text{H}\alpha$, but only two for $\text{H}\beta$).

Other spectral characteristics are the strong [O III] lines which are narrower than $\text{H}\beta$, weak Fe II emission, the presence of He I $\lambda 5876$, [O I] $\lambda 6300$, [Fe X] $\lambda 6374$, and [S II] $\lambda 6717$ at the red end of the observed spectrum.

Comparing the broad and narrow components of the Balmer lines, the flux arising from the BLR is approximately 15 times the flux from the NLR, and the line ratios lie in the AGN region of the diagnostic diagrams (Fig. 3). The large [O III]/ $\text{H}\beta$ line ratio of 10.88 indicates the strength of the ultraviolet AGN continuum. However, the $\text{H}\alpha/\text{H}\beta$ ratio (7.83) is also the highest in the sample, denoting a large amount of intrinsic reddening (see Tables 4 and 5).

The [O III] FWHM has a value of only 200 km s^{-1} . Hence the BH mass estimated from the [O III] FWHM ($4 \times 10^6 M_{\odot}$) is rather humble for a Seyfert galaxy, and it is also a factor approximately 44 smaller than the mass estimated from the $\text{H}\beta$ width (Table 6). The size for the BLR, estimated from the monochromatic 5100 \AA and the $\text{H}\beta$ broad component luminosities, is large (≈ 160 light days) and it is comparable to the sizes estimated for QSOs.

5.5. SBS 1136+595

This object is a 2MASS source. It was classified as a Sy 1 galaxy by Markarian et al. (1983), but appears as a NLS1 galaxy in the SBS. The Fe II is strong and, after subtraction, it is possible to detect a very noisy He II $\lambda 4686$ (Fig. 6). The FWHM of this line is poorly estimated, yielding a value of 10240 km s^{-1} (8700 km s^{-1} for the Lorentzian fit). This width may seem too large when compared with 1490 km s^{-1} measured for the FWHM of $\text{H}\beta$, but it is worth to remember (see discussion on SBS 1118+541 above) that the He II $\lambda 4686$ line shows negligible delays with respect to the continuum, and hence probably arises from fast moving BLR clouds very close to the central BH.

$\text{H}\alpha$ and $\text{H}\beta$ can be fitted using either two Gaussian components (narrow and broad) or a single Lorentzian. but for the weaker $\text{H}\gamma$ a single Gaussian can also reproduce the line profile. When the Lorentzian profile is applied, the three Balmer lines observed have FWHM smaller than 2000 km s^{-1} . However, as in the case of SBS 1118+541 discussed previously,

the broad components for the Gaussian fits are much larger than the limit for NLS1 galaxies. The remarks about the classification of SBS 1118+541 given above are also applicable to SBS 1136+595.

Also, as in the case of SBS 1118+541, the NLR shows evidence of stratification. Thus, the $H\alpha$ and $H\beta$ narrow components have widths much larger than the forbidden lines, and the differences among the FWHM of the forbidden lines, in the range 350-540 km s^{-1} , are also large but not as much as in SBS 1118+541, probably due to the absence of the [Fe VII] and [Fe X] lines. The narrow components $H\alpha/H\beta$ ratio (4.24) and the reddening ($A_V = 0.88$) are larger than in SBS 1118+541, but still moderate for an AGN (Table 5). A comparison between the broad and narrow components of the Balmer lines shows that the BLR emits ~ 1.5 times the NLR. Other lines present in the spectrum are He II $\lambda 5876$, [N II] $\lambda\lambda 6548 - 6584$, and [S II] $\lambda\lambda 6717, 6731$.

As in SBS 1118+541, the line ratios also lie in the H II region of the diagnostic diagrams (Fig. 3), in accordance with the result reported by Veilleux & Osterbrock (1987) for NLS1 whose broad Balmer lines have been fitted with Gaussian profiles.

The BH mass estimated from the FWHM of the broad component of $H\beta$ and [O III] agree (Table 6). But again, as in SBS 1118+541, the logarithm of the BH mass in solar units calculated from the Lorentzian $H\beta$ profile (Table 3) and the continuum at 5100 \AA changes from 8.06 to 7.17, in accordance with the NLS1 masses reported by Bian & Zhao (2004).

5.6. SBS 1204+505B and companion

SBS 1204+505B is a ROSAT and 2MASS source. In the SBS catalogue, it is classified as a Sy 1.8 galaxy. The object probably belongs to a compact group of three galaxies. Relative to the center of SBS 1204+505B, one galaxy is roughly to the south and the other to the west. The SDSS image from the former galaxy is unlikely to correspond to an AGN (no spectrum is available for this galaxy). On the contrary, the later galaxy shows a bright stellar-like nucleus which indicates some kind of nuclear activity. We refer to this galaxy as the *companion*. The spectra for both SBS 1204+505B and its companion are also available through the SDSS.

The reported B magnitude of SBS 1204+505B in the SBS catalogue is 17.0 ± 0.5 . In Table 1 the magnitude has been transformed from the SDSS photometric data (g' and r' bands) to allow comparison with the companion galaxy. The equation for the transformation is borrowed from Smith et al. (2002):

$$B = g' + 0.47(g' - r') + 0.17 \quad (18)$$

being the SDSS magnitudes g' and r' 16.18 and 15.57 for the SBS object, and 16.67 and 16.15 for the companion.

The spectrum of SBS 1204+505B does not show any Fe II blends. In the SDSS spectrum it is possible to distinguish a weak broad component of $H\beta$, but the spectrum presented in this paper shows only a narrow component. [O III] $\lambda\lambda$ 4959, 5007 lines are clearly visible ([O III]/ $H\beta$ = 2.27, see Table 4). There is evidence for the presence of the [O I] λ 6300 line, although it is below the detection level of our spectrum. [N II] $\lambda\lambda$ 6548, 6584 lines are clearly distinguished at both sides of the narrow component of $H\alpha$. The broad component of $H\alpha$ has a FWHM of about 3400 km s⁻¹, and its emission is comparable with that of the narrow component. Finally, at the red end of the spectrum the [S II] $\lambda\lambda$ 6717, 6731 lines can be clearly distinguished.

The narrow components $H\alpha/H\beta$ ratio has a value of 5.02, indicating an important amount of intrinsic reddening ($A_V = 1.35$). The BH mass estimated from the [O III] FWHM is $\sim 2 \times 10^8 M_\odot$.

The loci of all the emission line ratios in the diagnostic diagrams (Fig. 3) are in the AGN domain. The spectrum presented in this paper is consistent with that of a Sy 1.9, in contrast with both the SBS catalogue and the SDSS spectrum, which favor a Sy 1.8 classification. Of course, the classification may depend on the S/N ratio of the different spectra as well as the somewhat subjective detection threshold for the broad component. However, Penston & Perez (1984) have shown that large variations in the broad components of the Balmer lines are possible, and the same object may be classified as Sy 1 or Sy 2 nuclei in different epochs. Thus, the possibility that the object shows some kind of variability cannot be discarded.

About the companion, it is separated 33'' from the SBS object. The systemic velocity difference between both galaxies is 420 ± 30 km s⁻¹. With respect to the permitted lines, only $H\alpha$ and $H\beta$ are observed. Although both of them are narrow, $H\beta$ is more than twice broader than $H\alpha$. The $H\alpha/H\beta$ ratio is rather large (7.40, see Table 4), indicating that intrinsic reddening is important ($A_V = 1.35$) and the optical depth is larger than the thin limit ($\tau > 1$; see Table 5). He I λ 5876 is probably present but below the level of 3σ detection. For the forbidden lines, the [N II] pair is observed and these lines have similar FWHM to that of $H\alpha$, but the [S II] profiles are significantly broader. [O III] λ 5007 is probably present but below the 3σ detection level, as is [O I] λ 6300. These oxygen lines are also very weak in the SDSS spectrum.

The visual aspect (bright nucleus) and a glance to the narrow line spectrum suggest that the companion is a SBN. However, the line ratios are not well determined and two of three upper limits are compatible with both H II regions and low activity AGN (see Fig. 3). Only the [N II]/H α upper limit is incompatible with an AGN. The FWHM of H β (450 km s $^{-1}$) is too broad for a SBN or a H II region, although the line is weak (it is barely detected at the 3σ level) and all the other lines have FWHM less than 300 km s $^{-1}$. Following Osterbrock (1989), the [S II] λ 6717/[S II] λ 6731 line ratio (1.3) yields an electron density $\simeq 100$ cm $^{-3}$ (for a range of temperatures between 5000 and 2×10^4 K) which is typical for the spread-out giant H II regions. Thus, the companion galaxy can be classified as a SBN.

5.7. SBS 1340+569

This object is a ROSAT and 2MASS source, and it is classified as a Sy 1.8 galaxy in the SBS catalogue. It has an emission line neighbor galaxy located 4 m 4 to the East and 14" to the South. The SDSS image for this neighbor does not show a star-like nucleus, and the spectra show that both objects share the same redshift (0.04) and that the neighbor is probably a SB galaxy.

The spectrum of SBS 1340+569 does not show any Fe II blends, which favors the detection of the He II λ 4686 line. The intensity of the broad components of H α and H β are approximately twice the strength of the narrow components. The H β components are significantly wider than those of H α . The narrow components H α /H β ratio (3.26) almost matches the intrinsic value accepted for AGNs (3.1), indicating a very low intrinsic reddening (Table 5).

The He I 5876 line is very weak, and the measured FWHM for this line (680 km s $^{-1}$) is probably inaccurate. The [O III] lines are clearly visible ([O III]/H $\beta \gtrsim 3$), although these lines are narrower than H β . [O I] λ 6300 is also present, and it has a FWHM similar to [O III]. The [Fe X] λ 6374 is much broader than the other observed narrow lines (1560 km s $^{-1}$), as in the case of SBS 1118+541. The [N II] lines are weak ([N II]/H $\alpha = 0.23$), but they can be distinguished superposed to the broad H α component. These lines and the narrow H α component have similar widths (around 110 km s $^{-1}$).

The size of the BLR estimated from the continuum at 5100 Å and the broad component of H β luminosities are small, around 6 light days. This feature, along with the X-ray emission detected by ROSAT and the small amount of reddening measured, probably makes of this object a good candidate for reverberation mapping studies.

The presence of broad components confirms that this is an AGN. The [O III]/H β line

ratio ($\gtrsim 3$) indicates an ultraviolet excess probably associated to the AGN. The BH mass calculated from the $H\beta$ and $[O\ III]$ widths agree in an estimate of approximately $10^7 M_{\odot}$. Fig. 5 shows the strong correlation between the FWHM and the critical density for each forbidden line present in SBS 1340+569. This correlation shows that the velocities v of the clouds scale as $v \propto n_e^{0.23 \pm 0.01}$. This is a rather large dependency compared to M81 (Filippenko & Sargent 1988) or SBS 118+541, and it may indicate the presence of a starburst component that contributes to the low-excitation and lower critical density lines. Besides, some of the FWHM of the narrow lines are smaller than the value of 300 km s^{-1} that separates H II regions from AGN, while some are larger than this value (Table 2). Of the two line ratios plotted in the diagnostic diagrams (Fig. 3; note that the $[S\ II]$ lines are not in the range of the available spectrum), one lies in the AGN region while the other in the H II region. These features suggest that this object has a composite spectrum, and should be considered as a Seyfert (probably a Sy 1.8) with a SBN component.

5.8. SBS 1626+554

This object is an infrared (2MASS) and X-ray (ROSAT and EINSTEIN) source. Its spectrum clearly corresponds to a QSO, and the only forbidden lines observed are the $[O\ III]$ $\lambda\lambda 4959, 5007$. The permitted lines do not show narrow components, but two broad components are necessary to fit the Balmer lines, whose profiles are slightly asymmetric because the broadest component is systematically redshifted.

The $H\gamma$ profile is complicated because it is blended with the $[O\ III]$ $\lambda 4363$ line. As shown in Fig. 7, the broadest component of $H\gamma$ is redshifted by $\simeq 1000\text{ km s}^{-1}$. A similar redshifted component can be measured in $H\beta$, as shown in Fig. 8 and $H\alpha$. The extreme of the red wing of the $H\alpha$ profile is bitten by the telluric absorption band between 7570 and 7700 \AA . All these lines show a fit which is not as good near the peak as in the rest of the line, suggesting the presence of a narrow component, however, too weak to be measured with confidence ($S/N \sim 1.5$).

Apart from the Balmer lines, the only permitted lines observed are He II $\lambda 4686$ (after subtracting the Fe II blends), a feature identified as He I $\lambda 5048$, and He I $\lambda 5876$ which is easily recognized in the spectrum.

The broad line referred as He I $\lambda 5048$ deserves a especial remark. This feature is clearly seen as the reddest line in Fig. 8. The He I denomination is suggested because the measured gravity center of the line in the QSO rest-frame is at $\lambda 5051 \pm 3\text{ \AA}$ and, moreover, there are also other He I and He II lines detected in the spectrum. However, other atomic ions have

also permitted lines that dwell in the same region. Peterson et al. (1985) found a emission line at 5050 Å in Akn 120 that Crenshaw & Peterson (1986) proposed to be Si II λ 5056 or perhaps Si II λ 5041. A similar feature was also reported by Sergeev et al. (1997) in the spectrum of NGC 5548.

An indication of the temperature and density in the NLR can be obtained from the [O III] lines. Following Osterbrock (1989), the sum of the [O III] λ 4959 and [O III] λ 5007 fluxes divided by the [O III] λ 4363 flux has a value of 7.35, which indicates either a high temperature ($\lesssim 10^5$ K for $N_e < 10^7$) or most probably a high electron density (1.4×10^4 K for $N_e \sim 10^7$).

Finally, the BH mass estimated from the H β and [O III] line widths approximately agree within a factor of 2 ($M_{BH} = 8$ and $4 \times 10^8 M_\odot$, respectively, see Table 6).

6. Conclusions

Spectroscopic observations of 8 SBS extragalactic sources, as well as one companion galaxy, have been made using the OAN 2.1-m telescope at San Pedro Mártir, Mexico. The spectra in all but one case (SBS 0944+540) covers the rest frame H β and H α regions with a spectral resolution of 4.5 Å. The data has been corrected for redshift and for galactic extinction in order to derive spectrophotometric parameters and line ratios.

The spectra have been analyzed in detail and several faint emission lines have been measured. Any feature that strongly suggests the presence of an emission line was also reported. Fe II blends have been subtracted and their EW measured. These subtractions have allowed a better estimate of the emission lines parameters for H β and the [O III] λ 4959, 5007. Frequently, the Fe II subtraction has also made possible the identification and measurement of He II λ 4686 and, in one case, a feature that is identified as He I λ 5048.

Gaussian profiles were used to fit both the broad and the narrow emission lines. In most cases, a single component was used, except for the Balmer lines, which usually presented a narrow as well as one or more broad components. Some line profiles can also be described using Lorentzian fits with a lesser number of components. In these cases, the Lorentzian parameters for the broad lines have been reported.

Emission line FWHM and line ratios have been used, along with diagnostic diagrams, to separate AGNs from H II regions-like. Thus it was possible to review the classification of all objects. In two cases, a revised classification is proposed.

The analysis of the spectra reveal that the widths of the lines frequently change along

the spectral range, an effect that may imply a stratification of the NLR.

Intrinsic reddening, $B-V$ color excess, A_V extinction coefficients and optical depths for the V band, and at wavelengths corresponding to $H\alpha$, $H\beta$ and 5100 \AA , were calculated for all the objects with narrow Balmer components, and assuming that the local reddening has a continuous distribution along the line of sight and that the optical properties of the dust in the host-galaxy are the same as in the solar neighborhood.

Several parameters of the central black hole have been calculated with different methodologies and the results are compared. The mass of the central supermassive black hole has been inferred from its correlation with both the bulge stellar velocity dispersion (measured from the $[\text{O III}] \lambda 5007$ FWHM), and from the luminosity and FWHM of $H\beta$. The luminosity has been estimated from both the monochromatic flux at 5100 \AA and the integrated flux of the broad $H\beta$ component.

Below is a summary of the main topics discussed for each object:

- SBS 0848+526 is a reddened SBN which has a plume extending to a brighter neighbor Seyfert galaxy. The plume emits $H\alpha$, $H\beta$ and $[\text{O III}]$ lines.
- SBS 0944+540 is a QSO with strong Fe II blends and without evidence of narrow lines. The $H\beta$ profile is strongly asymmetric and shows a large blue bump and extended wings.
- SBS 1118+541 and 1136+595 are NLS1 which present many similarities. Both show discrepancies in the FWHM of the broad Balmer components used for their classification, depending on whether they were fitted using Gaussian or Lorentzian profiles. Their line ratios calculated from the Gaussian fits correspond to H II regions-like. There are differences in the widths among all the narrow lines, and particularly the narrow Balmer components are much broader than the forbidden lines, suggesting a stratification of the NLR. Both objects show low amounts of reddening and the masses of their black holes, estimated from the Lorentzian fit for $H\beta$, are one order of magnitude below the mass estimation from the Gaussian fit or from the $[\text{O III}]$ FWHM.
- SBS 1136+594 is a Sy 1.5 galaxy showing a large amount of reddening. The mass of the black hole estimated from the $[\text{O III}]$ FWHM is rather low for a Sy 1.5 and a factor 44 times smaller than the mass calculated from the $H\beta$ FWHM.
- SBS 1204+505B is an AGN with at least one companion galaxy, and is more probably a member of a compact group. The nucleus is reddened, and, in contrast with $H\alpha$, the broad component of $H\beta$ is not detected in the spectrum presented in this paper.

This feature leads to classify the object as a Sy 1.9, rather than a Sy 1.8 as proposed in the SBS catalogue. The companion of SBS 1204+505B reported in this paper is a very reddened SBN. However, the weak $H\beta$ line has a FWHM of 450 km s^{-1} , which is larger than the width expected for this kind of objects.

- SBS 1340+569 is probably a Sy 1.8 galaxy with a SBN component. The diagnostic plots for the available line ratios cover both the AGN and H II region domains. Besides, there is a variety of line widths for different ions and between the broad and narrow components of $H\alpha$ and $H\beta$, being the widths of the narrow lines in the $H\alpha$ region rather small for an AGN. The amount of reddening is small, as well as the size estimated for the BLR (~ 6 light days).
- SBS 1626+554 is a QSO whose permitted lines need two broad profiles to be fitted. The broadest component is redshifted by about 1000 km s^{-1} . Narrow components are suggested for all these three lines, but their S/N are too low to be measured reliably. The He II $\lambda 4686$ is discernible after the subtraction of the strong Fe II blends. A peculiar broad emission line, probably He I $\lambda 5048$, is observed and its parameters measured.

The author thanks the SPM staff, in particular to Felipe Montalvo and Juan Gabriel García, for their excellent assistance and technical support at the 2.1-m telescope. Jivan Stepanian suggested a list of interesting SBS objects. Luc Binette the anonymous referee made valuable comments that helped to improve to the manuscript. This work was supported by the *DGAPA-UNAM* grant IN113002.

The software system Image Reduction and Analysis Facility (IRAF) is distributed by the National Optical Astronomy Observatories, which are operated by the Association of Universities for Research in Astronomy, Inc., under cooperative agreement with the National Science Foundation.

This research has made use of the NASA/IPAC Extragalactic Database (NED) which is operated by the Jet Propulsion Laboratory, California Institute of Technology, under contract with the National Aeronautics and Space Administration.

REFERENCES

- Antonucci, R. 1993, *ARA&A*, 31, 473
- Antonucci, R. R. J., & Miller, J. S. 1985, *ApJ*, 297, 621

- Baldwin, J. A., Phillips, M. M., & Terlevich, R. 1981, *PASP*, 93, 5
- Baldwin, J., Ferland, G., Korista, K., & Verner, D. 1995, *ApJ*, 455, L119
- Balzano, V. A. 1983, *ApJ*, 268, 602
- Bian, W., & Zhao, Y. 2004, *MNRAS*, 347, 607
- Bian, W.-H., Cui, Q.-L., & Chao, L.-H. 2006a, *Chin. J. Astron. Astrophys.*, 6, 281
- Bian, W., Yuan, Q., & Zhao, Y. 2006b, *MNRAS*, 367, 860
- Binette, L., Wang, J., Villar-Martin, M., Martin, P. G., & Magris C., G. 1993, *ApJ*, 414, 535
- Bischof, O. B., & Becker, R. H. 1997, *AJ*, 113, 2000
- Boller, T., Brandt, W. N., & Fink, H. 1996, *A&A*, 305, 53
- Botte, V., Ciroi, S., di Mille, F., Rafanelli, P., & Romano, A. 2005, *MNRAS*, 356,
- Blumenthal, G. R., & Mathews, W. G. 1975, *ApJ*, 198, 517
- Cardelli, J. A., Clayton, G. C., & Mathis, J. S. 1989, *ApJ*, 345, 245
- Crenshaw, D. M., & Peterson, B. M. 1986, *PASP*, 98, 185
- de Robertis, M. M., & Osterbrock, D. E. 1984, *ApJ*, 286, 171
- Dietrich, M., Crenshaw, D. M., & Kraemer, S. B. 2005, *ApJ*, 623, 700
- Dumont, A. M., & Collin-Souffrin, S. 1990a, *A&AS*, 83, 71
- Dumont, A. M., & Collin-Souffrin, S. 1990b, *A&A*, 229, 313
- Espey, B. R., et al. 1994, *ApJ*, 434, 484
- Ferguson, J. W., Korista, K. T., Baldwin, J. A., & Ferland, G. J. 1997, *ApJ*, 487, 122
- Ferrarese, L., & Merritt, D. 2000, *ApJ*, 539, L9
- Ferrarese, L., Pogge, R. W., Peterson, B. M., Merritt, D., Wandel, A., & Joseph, C. L. 2001, *ApJ*, 555, L79
- Filippenko, A. V., & Halpern, J. P. 1984, *ApJ*, 285, 458
- Filippenko, A. V., & Sargent, W. L. W. 1985, *ApJS*, 57, 503

- Filippenko, A. V., & Sargent, W. L. W. 1988, *ApJ*, 324, 134
- Gaskell, C. M. 1982, *PASP*, 94, 891
- Gaskell, C. M., & Ferland, G. J. 1984, *PASP*, 96, 393
- Gebhardt, K., et al. 2000, *ApJ*, 539, L13
- Gonçalves, A. C., Véron-Cetty, M.-P., & Véron, P. 1999, *A&AS*, 135, 437
- Goodrich, R. W. 1989, *ApJ*, 342, 224
- Halpern, J. P., & Steiner, J. E. 1983, *ApJ*, 269, L37
- Heckman, T. M. 1980, *A&A*, 87, 152
- Hewitt, A., & Burbidge, G. 1989, *A New Optical Catalog of Quasi-Stellar Objects*, Univ. of Chicago Press, Chicago
- Ho, L. C., Filippenko, A. V., Sargent, W. L. W., & Peng, C. Y. 1997, *ApJS*, 112, 391
- Jiménez-Bailón, E., Santos-Lleó, M., Dahlem, M., Ehle, M., Mas-Hesse, J. M., Guainazzi, M., Heckman, T. M., & Weaver, K. A. 2005, *A&A*, 442, 861
- Jiménez-Bailón, E., Santos-Lleó, M., Mas-Hesse, J. M., Guainazzi, M., Colina, L., Cerviño, M., & González Delgado, R. M. 2003, *ApJ*, 593, 127
- Kaspi, S., Smith, P. S., Netzer, H., Maoz, D., Jannuzi, B. T., & Giveon, U. 2000, *ApJ*, 533, 631
- Kaspi, S., Maoz, D., Netzer, H., Peterson, B. M., Vestergaard, M., & Jannuzi, B. T. 2005, *ApJ*, 629
- Kauffmann, G., et al. 2003, *MNRAS*, 346, 1055
- Kewley, L. J., Groves, B., Kauffmann, G., & Heckman, T. 2006, *astro-ph/0605681*
- Kewley, L. J., Heisler, C. A., Dopita, M. A., & Lumsden, S. 2001, *ApJS*, 132, 37
- Leighly, K. M. 1999, *ApJS*, 125, 317
- Markarian, B. E., Lipovetskii, V. A., & Stepanian, D. A. 1983, *Astrofizika*, 19, 29
- Martel, A., & Osterbrock, D. E. 1994, *AJ*, 107, 1283
- Marziani, P., Zamanov, R. K., Sulentic, J. W., & Calvani, M. 2003, *MNRAS*, 345, 1133

- Moran, E. C., Halpern, J. P., & Helfand, D. J. 1996, *ApJS*, 106, 341
- Nelson, C. H., & Whittle, M. 1996, *ApJ*, 465, 96
- Nelson, C. H. 2000, *ApJ*, 544, L91
- Netzer, H. 1982, *MNRAS*, 198, 589
- O'Donnell, J. E. 1994, *ApJ*, 422, 158
- Onken, C. A., Ferrarese, L., Merritt, D., Peterson, B. M., Pogge, R. W., Vestergaard, M., & Wandel, A. 2004, *ApJ*, 615, 645
- Osterbrock, D. E. 1989, in *Astrophysics of Gaseous Nebulae and Active Galactic Nuclei*, University Science Books, Mill Valley (CA), USA
- Osterbrock, D. E., & Koski, A. T. 1976, *MNRAS*, 176, 61P
- Osterbrock, D. E., & Pogge, R. W. 1985, *ApJ*, 297, 166
- Pelat, D., Alloin, D., & Fosbury, R. A. E. 1981, *MNRAS*, 195, 787
- Penston, M. V., & Perez, E. 1984, *MNRAS*, 211, 33P
- Peterson, B. M., Meyers, K. A., Carpriotti, E. R., Foltz, C. B., Wilkes, B. J., & Miller, H. R. 1985, *ApJ*, 292, 164
- Peterson, B. M. 1993, *PASP*, 105, 247
- Rodríguez-Ardila, A., Binette, L., Pastoriza, M. G., & Donzelli, C. J. 2000, *ApJ*, 538, 581
- Savage, B. D., & Mathis, J. S. 1979, *ARA&A*, 17, 73
- Schlegel, D. J., Finkbeiner, D. P., & Davis, M. 1998, *ApJ*, 500, 525
- Sergeev, S. G., Pronik, V. I., Malkov, Y. F., & Chuvaev, K. K. 1997, *A&A*, 320, 405
- Smith, J. A., et al. 2002, *AJ*, 123, 2121
- Stepanian, J. A. 2005, *Rev. Mexicana Astron. Astrofis.*, 41, 155
- Stepanian, J. A., Chavushyan, V. H., Carrasco, L., Valdés, J. R., Mújica, R. M., Tovmassian, H. M., & Ayvazyan, V. T. 2002, *AJ*, 124, 1283
- Storey, P. J., & Zeippen, C. J. 2000, *MNRAS*, 312, 813

- Sulentic, J. W., Marziani, P., & Dultzin-Hacyan, D. 2000, *ARA&A*, 38, 521
- Tremaine, S., et al. 2002, *ApJ*, 574, 740
- Ulrich, M.-H., & Horne, K. 1996, *MNRAS*, 283, 748
- Veilleux, S., & Osterbrock, D. E. 1987, *ApJS*, 63, 295
- Véron-Cetty, M.-P., Véron, P., & Gonçalves, A. C. 2001, *A&A*, 372, 730
- Whittet, D. C. B. 1992, in *Dust in the Galactic Environment*, Tayler, R. J. & White, R. E. eds, Institute of Physics Publishing, Bristol, UK
- Williams, R. J., Pogge, R. W., & Mathur, S. 2002, *AJ*, 124, 3042
- Wilson, A. S., & Heckman, T. M. 1985, *Astrophysics of Active Galaxies and Quasi-Stellar Objects*, 39
- Witt, A. N., Thronson, H. A., Jr., & Capuano, J. M., Jr. 1992, *ApJ*, 393, 611
- Zamanov, R., & Marziani, P. 2002, *ApJ*, 571, L77

Fig. 1.— Spectra of the SBS objects and the companion galaxy of SBS 1204+505B.

Fig. 2.— Transmittance values for the galactic extinction of SBS 1136+594. The squares show the transmittances obtained from the galactic extinction (eq. 2) for the UBVRIJHKL' band measurements extracted from NED. The continuous line corresponds to the exponential associate function fit (eq. 3).

Fig. 3.— Diagnostic diagram adapted from Kewley et al. 2006. The letter code for the objects is: A - SBS 0848+526, B - SBS 1118+541, C - SBS 1136+594, D - SBS 1136+595, E - SBS 1204+505B, F - Companion, and G - SBS 1340+569

Fig. 4.— Detail of the $H\beta$ region in SBS 1118+541. The continuous line shows the original data, and the dashed line the data after subtracting the Fe II blends. The He II $\lambda 4686$ (around 5170 \AA at the observer's frame) is clearly visible after the subtraction.

Fig. 5.— The common logarithm of the FWHM vs the critical density for collisional de-excitation (for a temperature of 10^4 K) reveals a highly significant correlation for SBS 1118+540 (filled squares) and SBS 1340+569 (open squares). The solid line shows the weighted linear fit for SBS 1118+540 (slope $b = 0.07 \pm 0.01$; correlation coefficient $r = 0.946$). Similarly, the dashed line shows the weighted linear fit for SBS 1340+569 ($b = 0.23 \pm 0.01$; $r = 0.997$).

Fig. 6.— Gaussian fit of the $H\beta$ region in SBS 1118+541 (upper panel) and SBS 1136+595 (lower panel). The continuous line shows the data after Fe II and continuum subtraction. The dotted lines show the individual components of the fit (He II $\lambda 4686$, $H\beta$ narrow and broad, and [O III] $\lambda 4959$ and 5007). Finally, the dashed thick line shows the profile obtained combining the individual components.

Fig. 7.— Fit of the $H\gamma$ line in SBS 1626+554. The continuous line shows the data after subtracting the continuum. The dotted lines show the individual components of the line and the narrow [O III] $\lambda 4363$, while the dashed thick line represents the complete fit. A narrow component, would help to improve the fit near the peak.

Fig. 8.— Fit of the region around $H\beta$ in SBS 1626+554. The continuous line shows the data after subtracting the Fe II blends and the continuum. The dotted lines show the individual components of the fit (He II $\lambda 4686$, the three broad components of $H\beta$, and [O III] $\lambda\lambda 4959, 5007$). The dashed thick line shows the complete fit. As in the previous figure, a weak narrow component would improve the fit near the peak.

Table 1. Log of observations

SBS designation	R.A. 2000	Dec. 2000	B	z em	M_B	Date dd-mm-yy	Spectral range	Spectral type ^a
0848+526 ^b	08 51 51.40	+52 28 25.2	17.5	0.064	-19.9	11-04-02	5000-7100	SBN
0944+540	09 47 55.94	+53 50 00.5	16.84	0.488	-25.5	14-04-02	6800-9000	QSO
1118+541	11 21 08.55	+53 51 20.7	16.41	0.103	-22.9	12-04-02 14-04-02	4800-7550 6500-8000	NLS1
1136+594	11 39 08.91	+59 11 54.5	16.26	0.060	-21.5	11-04-02	5000-7100	Sy 1.5
1136+595	11 39 00.48	+59 13 46.7	17.0	0.115	-22.1	12-04-02 14-04-02	4800-7580 6500-8000	NLS1
1204+505B ^b	12 06 55.55	+50 17 36.8	16.64 ^c	0.062	-21.3	13-04-02	5160-7210	<i>Sy 1.9</i>
(& Companion) ^d	12 06 52.40	+50 17 24.3	17.08 ^c	0.063	-20.8	13-04-02	5160-7210	<i>SBN</i>
1340+569 ^b	13 42 10.23	+56 42 11.6	16.98	0.040	-20.4	14-04-02	4800-7210	<i>Sy 1+SBN</i>
1626+554	16 27 56.11	+55 22 31.9	16.17	0.134	-23.4	12-04-02 14-04-02	4800-7580 6500-8000	QSO

^aNew or revised classification in italics.

^bPair.

^cCalculated from SDSS photometric database using the Smith et al. (2002) set of transformation equations.

^dA companion of SBS 1204+505B.

Table 2. Gaussian rest-frame EW and FWHM

Line identification	0848+526		0944+540		1118+541		1136+594		1136+595		1204+505B		Companion		1340+569		1626+554	
	EW	FWHM	EW	FWHM	EW	FWHM	EW	FWHM	EW	FWHM	EW	FWHM	EW	FWHM	EW	FWHM	EW	FWHM
H γ λ 4340	22	2420	31	4250
2nd component	4	1650
[O III] λ 4363	1	710
Fe II λ 4540	29	37	54	...
He II λ 4686	< 2	...	19	4690	33	10240	9	3560	13	5650
H β λ 4861n	17	210	19	1040	4	250	24	1050	6	520	5	450	9	400
H β λ 4861b	33	2630	53	4110	61	2920	44	4120	18	3430	61	8860
2nd component	81	2470	13	1720	65	3350
3rd component	112	13120
[O III] λ 4959	8	200	12	550	17	220	8	530	5	510	9	330	3	620
[O III] λ 5007	23	200	36	530	51	200	23	540	13	500	< 5	...	28	290	8	610
He I λ 5048	6	4340
Fe II λ 5300	101	...	46	...	34	...	43	78	...
He I λ 5876	4	170	8	5350	11	3990	6	1210	< 5	...	3	680	30	5460
2nd component	2	920
[Fe VII] λ 6087	2	1050	< 4
[O I] λ 6300	3	160	1	490	4	340	< 5	...	< 7	...	3	320
[Fe X] λ 6374	2	1230	3	330	6	1560
[N II] λ 6548	9	150	2	320	7	350	7	200	5	200	3	120
H α λ 6563n	116	150	90	870	32	320	140	1000	30	200	39	200	38	110
H α λ 6563b	220	2970	222	3210	176	4870	37	3390	80	2260	320	3220
2nd component	126	3600	289	6680
[N II] λ 6584	27	190	6	320	19	350	20	200	15	210	9	110
[S II] λ 6717	1	400	3	320	8	510	4	200	6	280
[S II] λ 6731	1	460	7	460	4	200	5	290

Table 3. Lorentzian rest-frame EW and FWHM

Line identification	0944+540		1118+541		1136+595	
	EW	FWHM	EW	FWHM	EW	FWHM
H γ λ 4340	28	1930
He II λ 4686	< 2	...	22	3270	42	8700
H β λ 4861b	157	2700	73	1510	73	1480
2nd component	65	3220
He I λ 5876	24	5220	13	1360
H α λ 6563b	355	1380	334	1340

Table 4. Gaussian narrow emission line ratios

SBS Designation	$\frac{[\text{O III}]\lambda 5007}{\text{H}\beta\text{n}}$	$\frac{\text{Fe II}\lambda 5300}{\text{H}\beta\text{n}}$	$\frac{[\text{O I}]\lambda 6300}{\text{H}\alpha\text{n}}$	$\frac{\text{H}\alpha\text{n}}{\text{H}\beta\text{n}}$	$\frac{[\text{N II}]\lambda 6584}{\text{H}\alpha\text{n}}$	$\frac{[\text{S II}]\lambda 6717}{\text{H}\alpha\text{n}}$
0848+526	1.41	...	0.03	6.84	0.24	...
1118+541	1.86	1.81	0.02	3.60	< 0.03	0.02
1136+594	10.88	6.53	0.11	7.83	0.20	0.09
1136+595	0.91	1.61	< 0.02	4.24	0.14	0.06
1204+505B	2.27	...	< 0.15	5.02	0.67	0.15
Companion	< 0.86	...	< 0.18	7.40	0.38	0.21
1340+569	3.09	...	0.08	3.26	0.23	...

Table 5. Reddening parameters

SBS	C	E_{B-V}	A_V	τ_V	τ_α	τ_β	τ_{5100}
0848+526	2.21	0.73	2.22	2.04	1.66	2.42	2.26
1118+541	0.42	0.14	0.42	0.39	0.31	0.46	0.43
1136+594	2.58	0.85	2.60	2.39	1.94	2.83	2.64
1136+595	0.87	0.29	0.88	0.81	0.65	0.96	0.89
1204+505B	1.34	0.44	1.35	1.25	1.01	1.47	1.38
Companion	2.42	0.80	2.44	2.25	1.82	2.66	2.48
1340+569	0.14	0.05	0.14	0.13	0.10	0.15	0.14

Table 6. Parameters of the black holes

SBS	$\log(L/L_{\odot})$		R_{BLR} (light days)		$\log(M_{\text{BH}}/M_{\odot})$			$\log\left(\frac{M_{\text{BH}(5100 \text{ \AA})}}{M_{\text{BH}([\text{O III}]])}\right)$
	5100 \AA	H β	5100 \AA	H β	5100 \AA	H β	[O III]	
0944+540 ^a	11.69	10.16	169.62	281.19	9.63	9.85
1118+541	11.07	9.13	63.21	54.54	8.19	8.13	8.34	-0.15
1136+594	11.62	9.84	151.18	166.90	8.28	8.32	6.64	1.64
1136+595	10.87	8.88	45.93	36.30	8.06	7.96	8.37	-0.31
1204+505B	10.70	6.82	35.23	8.24
1340+569	9.82	7.38	8.60	3.40	7.17	6.77	7.29	-0.12
1626+554 ^a	11.13	9.25	69.35	66.09	8.90	8.88	8.58	0.32

^aNot corrected for intrinsic reddening.

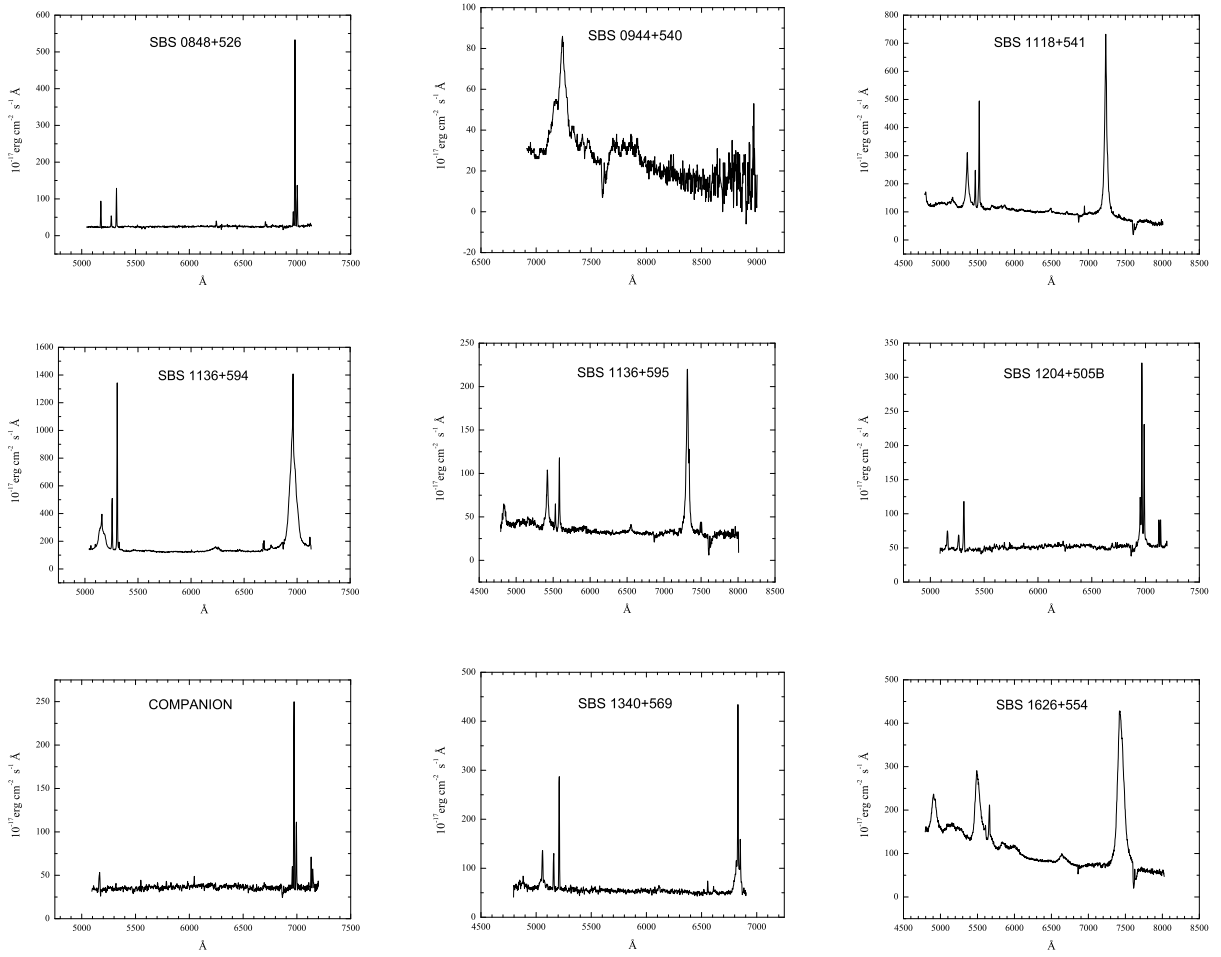


Fig. 1.—

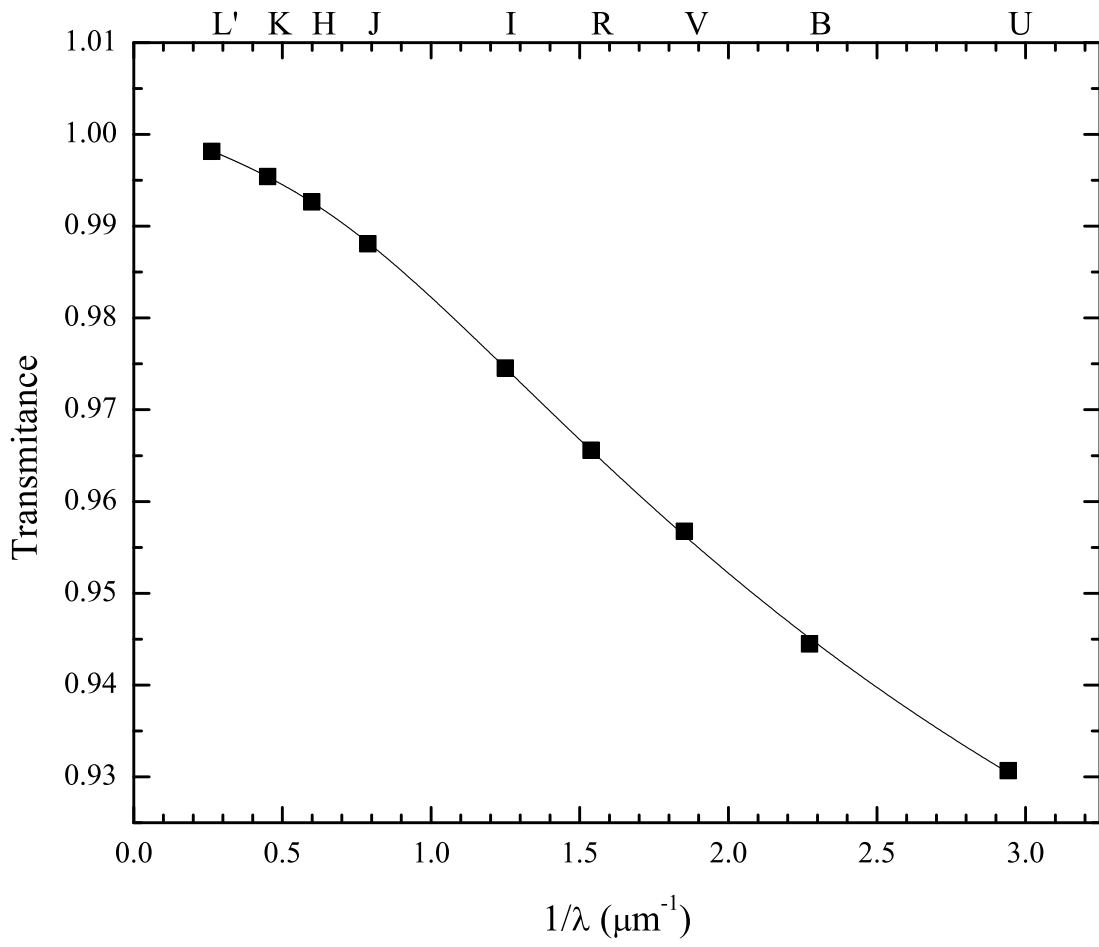


Fig. 2.—

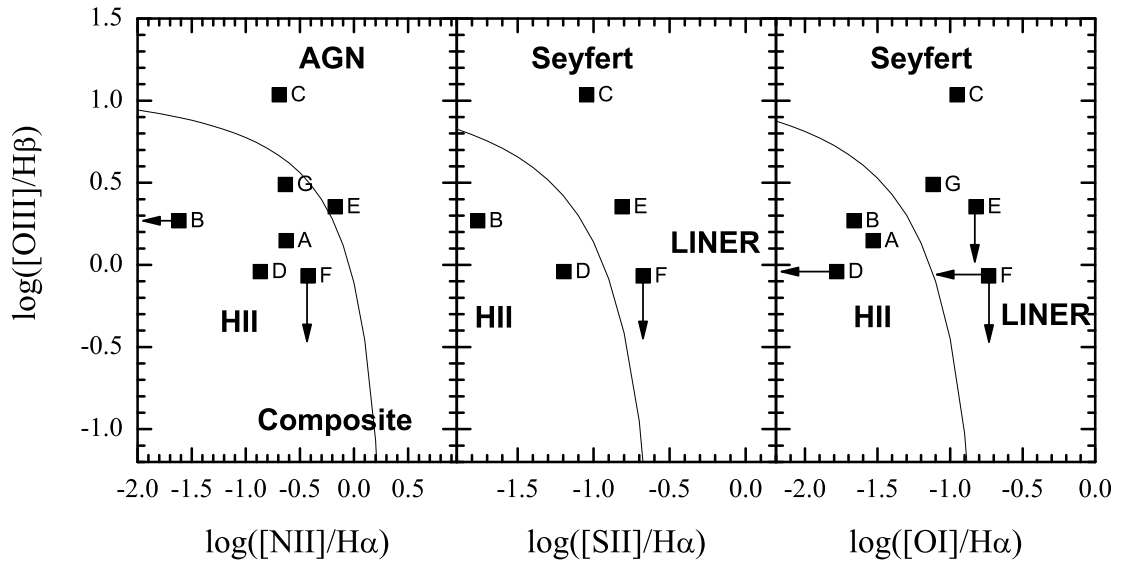


Fig. 3.—

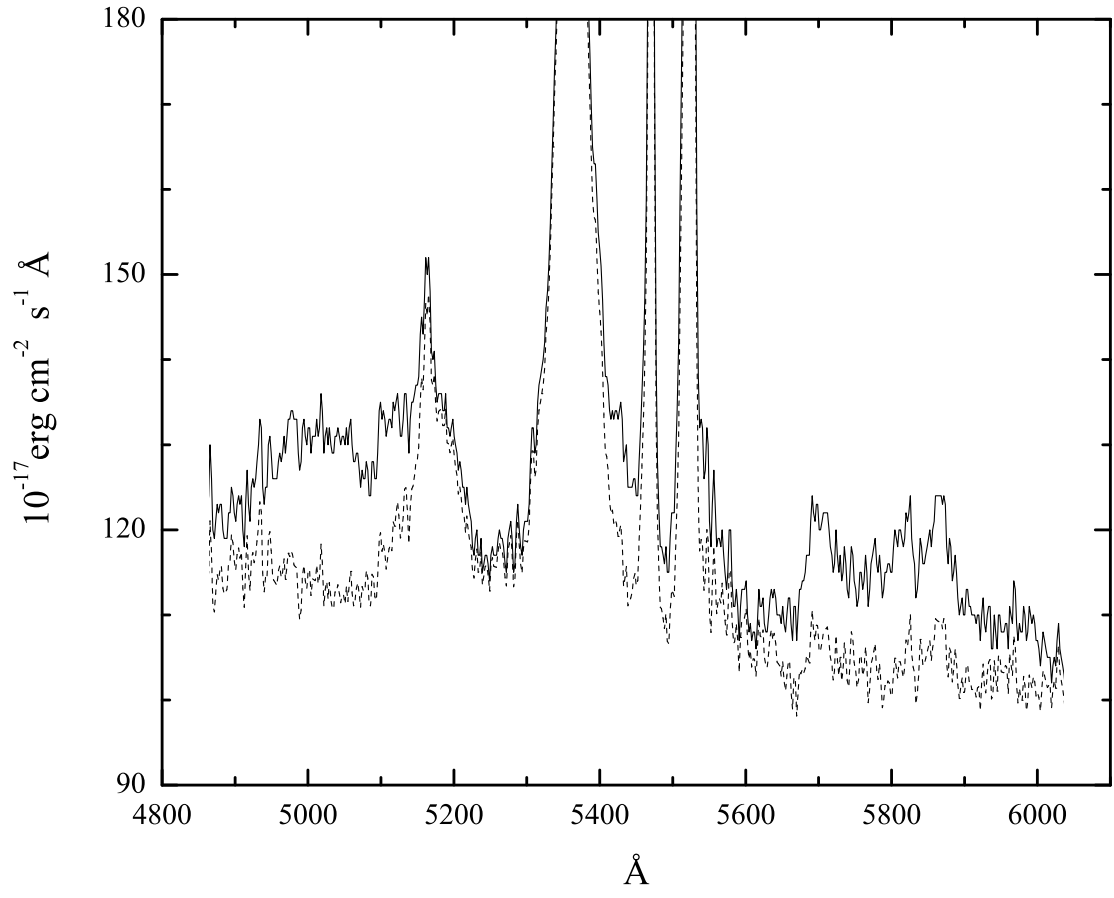


Fig. 4.—

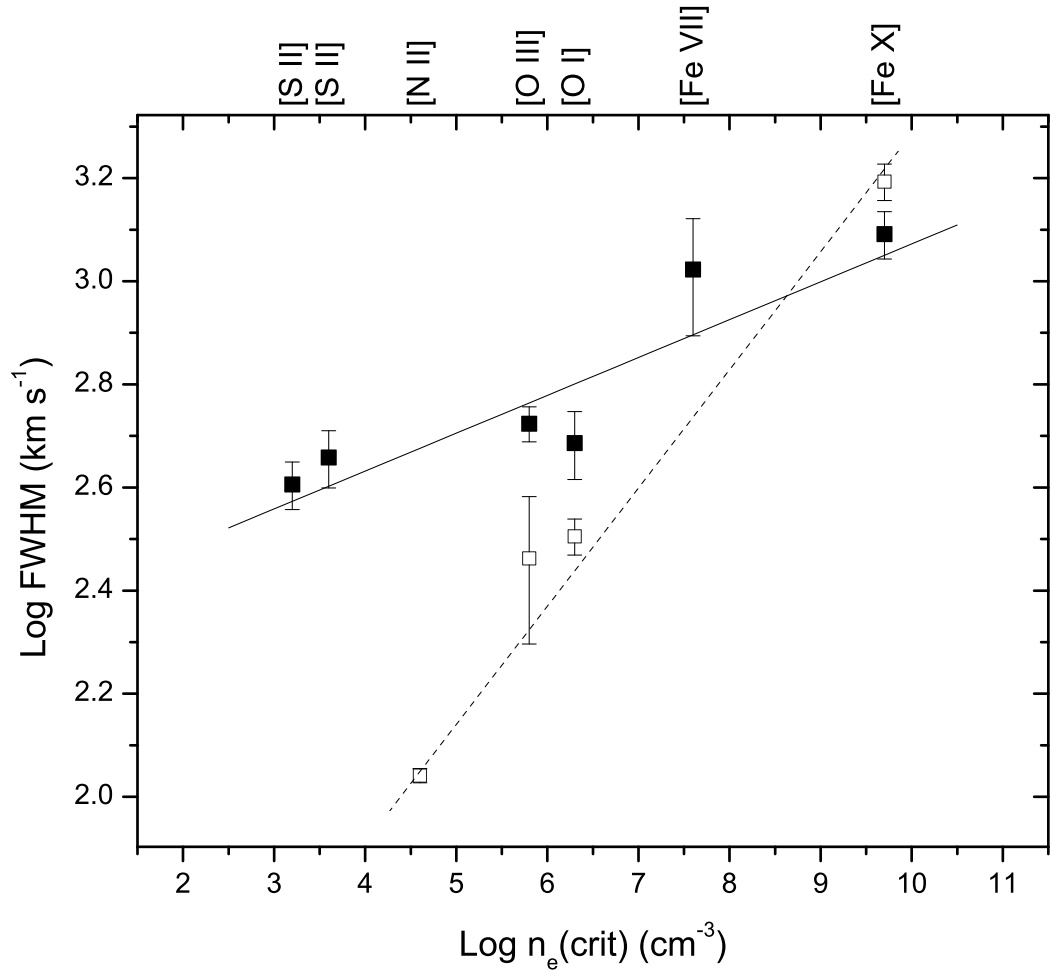


Fig. 5.—

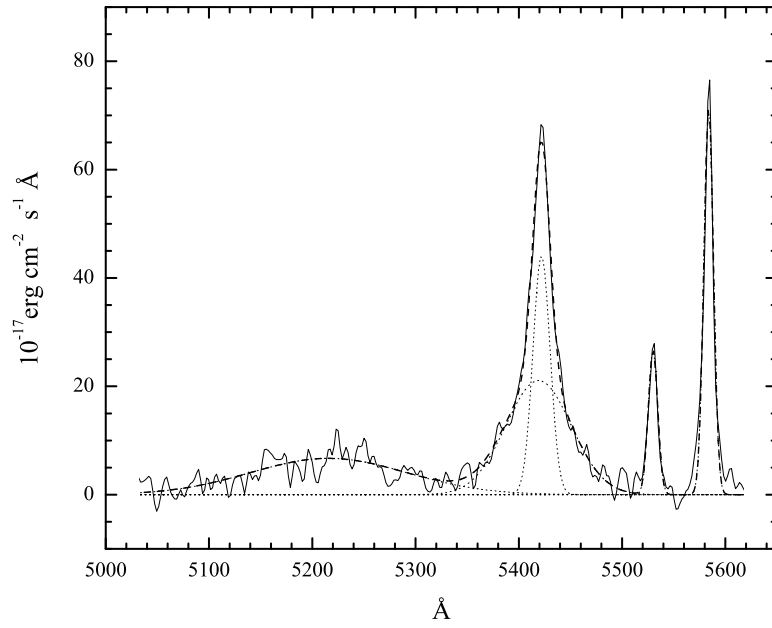
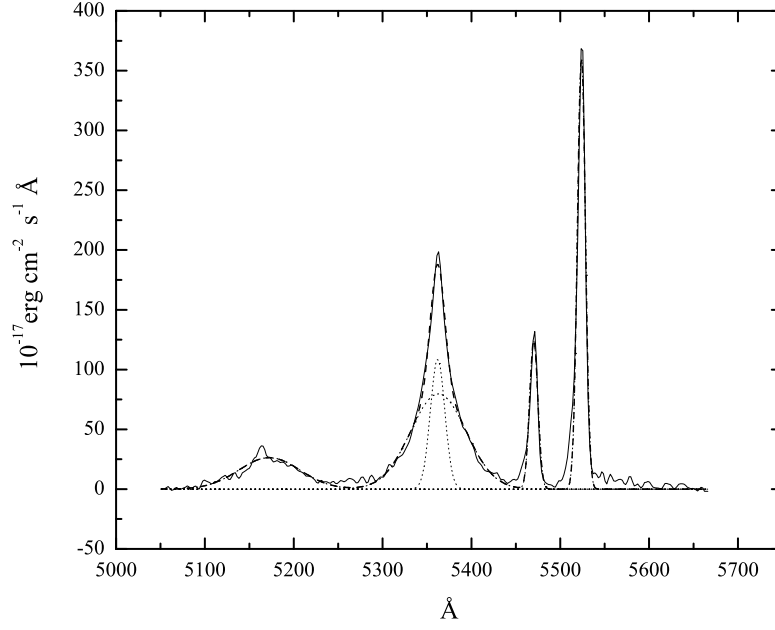


Fig. 6.—

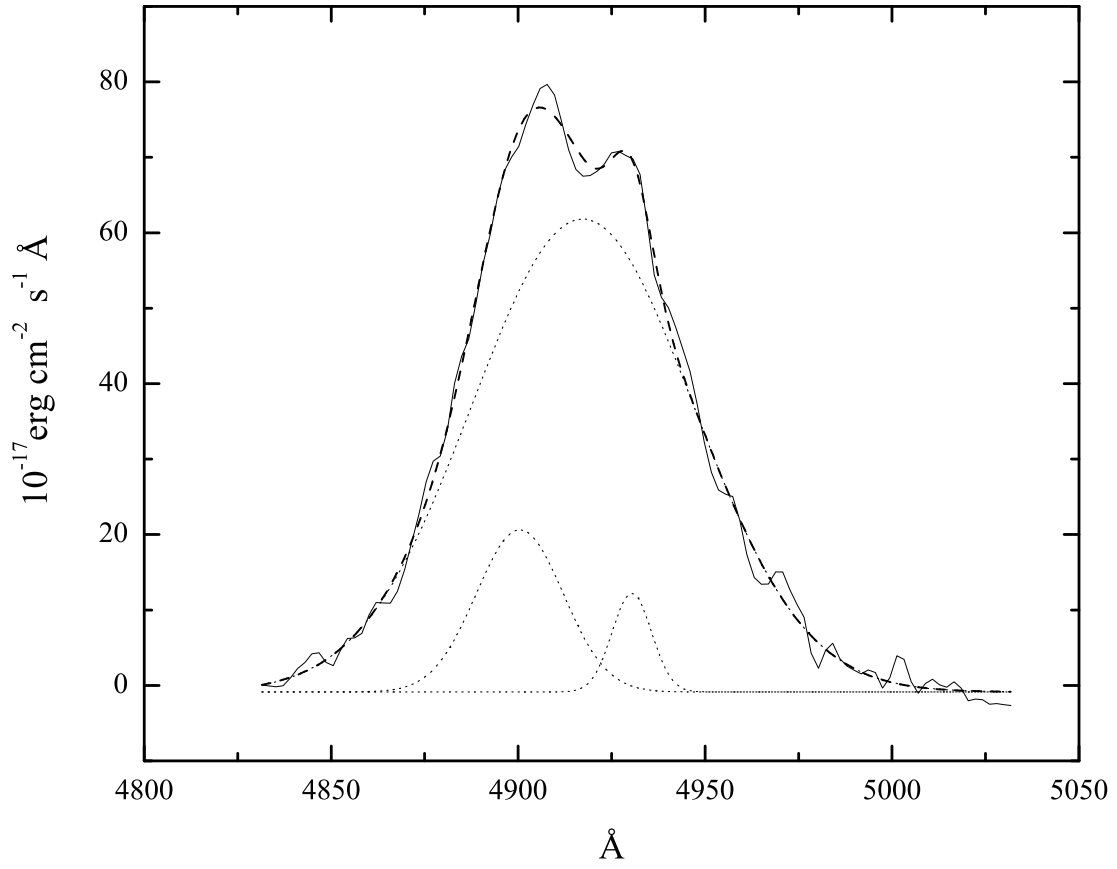


Fig. 7.—

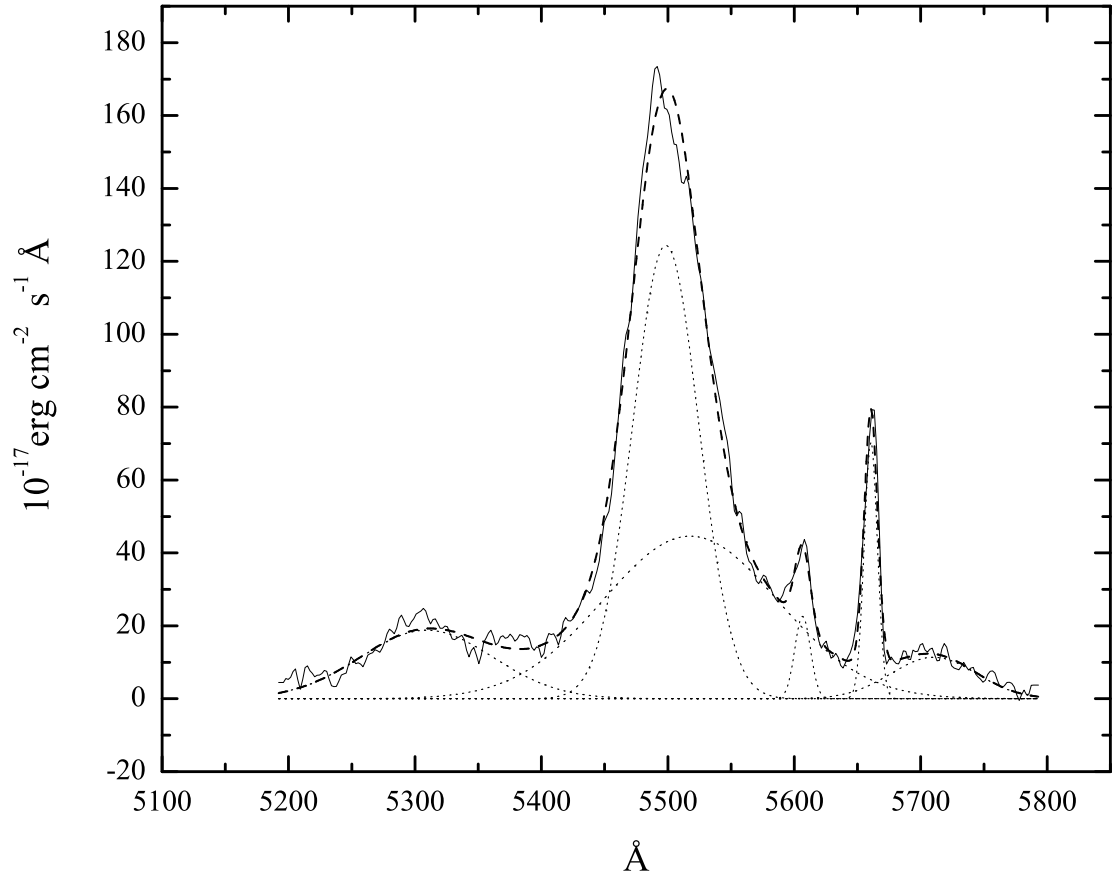


Fig. 8.—